Angewandte Chemie
Eine Zeitschrift der Gesellschaft Deutscher Chemiker

Supporting Information

Protonated Imine-Linked Covalent Organic Frameworks for Photocatalytic Hydrogen Evolution

*Jin Yang, Amitava Acharjya, Meng-Yang Ye, Jabor Rabeah, Shuang Li, Zdravko Kochovski, Sol Youk, Jérôme Roeser, Julia Grüneberg, Christopher Penschke, Michael Schwarze, Tianyi Wang, Yan Lu, Roel van de Krol, Martin Oschatz, Reinhard Schomäcker, Peter Saalfrank, and Arne Thomas**

anie_202104870_sm_miscellaneous_information.pdf
anie_202104870_sm_Video_1.mp4
anie_202104870_sm_Video_2.mp4

Table of Contents

Section S1. Materials and methods

1.1 Materials

All the reagents and solvents used for the synthesis were commercially available and used without further purification. The 1,4-dioxane (99.9%), mesitylene (1,3,5-trimethylbenzene, >98%) o-DCB (1,2-Dichlorobenzene, 99%) anhydrous n-BuOH (n-Butanol, 99%) were purchased from Sigma Aldrich Chemicals. Tta (2,4,6-Tris(4-aminophenyl)triazine, 95%), Tfa (Tris(4-formylphenyl)amine, >97.0%), Tpa-CHO (1,3,5-Tris(4-formylphenyl)benzene, >96.0%) and Tpa-NH2 (1,3,5-Tris(4-aminophenyl)benzene, >93.0%) were all supplied by TCI. Acetic acid (>99.0%) was purchased from Carl Roth. All chemicals were used without further purification.

1.2 Characterization

1.2.1 Powder X-ray diffraction (PXRD) analysis

Powder X-ray diffraction data was collected on a Bruker D8 Advance diffractometer in reflection geometry operating with a Cu Kα anode (λ = 1.54178 Å) operating at 40 kV and 40 mA. Samples were ground and mounted as loose powders onto a Si sample holder. PXRD patterns were collected from 2 to 60 2θ degrees with a step size of 0.02 degrees and an exposure time of 2 seconds per step.

1.2.2 Fourier transform infrared spectroscopy (FTIR) analyses

The Fourier transform infrared spectroscopy (FTIR) analyses of the samples were carried on Varian 640IR spectrometer equipped with an ATR cell.

1.2.3 NMR measurements

^{1}H NMR for the samples dissolved in suitable solvents were carried on Bruker Avance II 200. ^{13}C Solid state NMR (cross polarization magic-angle spinning (CP/MAS)) spectra were carried out on a Bruker Avance 400 MHz spectrometer operating at 100.6 MHz.

1.2.4 Solid-state diffuse reflectance Ultraviolet–visible spectroscopy (UV-DRS) analysis

Solid-state diffuse reflectance Ultraviolet–visible spectroscopy (UV-vis) spectra of the as pristine COF powders and starting monomers have been collected on Varian Cary 300 UV-Vis Spectrophotometer.

1.2.5 N_2 and Ar Physisorption measurements:

N_2 and Ar sorption measurements were performed on a volumetric sorption instrument (Autosorb-iQ-MP). Prior to the gas sorption studies of COFs, the samples were dried under a dynamic vacuum (<10^{-3} Torr) at room temperature (RT) followed by heating to 120 °C for 12 h. Using the N_2 adsorption isotherms, the surface areas were calculated over a pressure range 0.01-0.9 = p/p_0 using Brunauer-Emmett-Teller (BET), and pore size distributions were calculated using the quenched solid density functional theory (QSDFT) method on the Ar adsorption branch.

1.2.6 Scanning electron microscope (SEM)

The SEM analyses of COF samples were performed on an S-2700 scanning electron microscope (Hitachi, Tokyo, Japan).

1.2.7 Low-dose, high-resolution transmission electron microscopy (HRTEM)

COF samples for HRTEM were sonicated in ethanol for 10 min and a 4 µL of sample dispersion was applied to Lacey carbon-coated copper TEM grids (200 mesh, Science Services) and subsequently dried under a fume hood. The grids were loaded at room temperature into a cryogenic transfer holder (Gatan 914, Gatan, Munich, Germany) that was cooled with liquid nitrogen after the transfer to the TEM. Imaging was performed with a low dose acquisition scheme using SerialEM[1] on JEM-2100 (JEOL GmbH, Eching, Germany) operated at 200 kV and equipped with a 4 k × 4 k CMOS digital camera (TVIPS TemCam-F416). HRTEM images were acquired at a magnification of 500,000×, corresponding to a pixel size of 0.23 Å at the specimen level, while keeping the total electron dose below 10 e $Å^{-2}$. All imaging was carried out at temperatures around 90 K.

1.2.8 Electron paramagnetic resonance spectroscopy (EPR)

EPR measurements in X-band (microwave frequency ≈ 9.87 GHz) were performed at 293 K by a Bruker EMX CW micro spectrometer equipped with an ER 4119HS-WI high-sensitivity optical resonator with a grid in the front side. The samples were illuminated by a 300 W Xe lamp with 420 nm cut-off filter (LOT Oriel). All the samples were measured under the same conditions (microwave power: 6.74 mW, receiver gain: 2×10^4, modulation frequency: 100 kHz, modulation amplitude: 3 G, Sweep time: 45 s). g values have been calculated from the resonance field B_0 and the resonance frequency v using the resonance condition $hv = g\beta B_0$. The calibration of the g values was performed using DPPH (2, 2-diphenyl-1- picrylhydrazyl) (g = 2.0036 ± 0.00004).

1.2.9 Water Sorption Measurements

Water physisorption were measured at 298 K on a Quantachrome Autosorb IQ instrument. Prior to the measurements, the samples (weight ~50 mg) were degassed under vacuum at 120 °C for 15 h.

1.2.10 Photoluminescence spectra and time-correlated single photon counting (TCSPC)

A Picoquant PicoHarp 300 histogrammer was used for PL measurements. Samples were excited with a Picoquant 405 nm pulsed laser diode with power of 1 µW and a laser spot size of 10 µm. PL light was focused onto a multimode fiber (50 µm core diameter) with lens L3 and the fiber is connected to a detector assembly where luminescence was detected by MPD Si APD detector. The detection wavelength is larger than 450 nm.

1.3 Quantum chemical calculations

All calculations were performed using ORCA,[21] version 4.0.0.2. We used cluster models built from the experimentally determined structures which contained one pore (i.e., three Tta and three Tfa units), with dangling bonds connecting to neighboring clusters saturated by hydrogens as shown in Figure S14 and Figure S15. For protonated species, we used a model with one protonated imine group (TtaTfa+H^+) and one with all six imine groups protonated (Tta-Tfa-+$6H^+$), the latter as an extreme case. Only the protonated imine groups were geometry-optimized while all other atoms were kept fixed. This optimization was done with the PBE functional[22] and the D3 dispersion correction[23] with Becke-Johnson damping,[24] using the 6-311G** basis set.[25] CAM-B3LYP[26–29] calculations were performed using the def2-SVP basis set,[30] which gives very similar results compared to the larger 6-311G** basis set. Time-dependent density functional theory (TD-DFT)[31] was used to calculate excitation energies and oscillator strengths. Natural transition orbitals (NTOs)[32] were used to analyse the electron-hole pairs contributing to the excitations. The TD-DFT excitation energies give a more realistic description than HOMO-LUMO gaps when compared to experimental UV-Vis spectra.

Section S2. Synthesis of the COFs

Generally, all the COFs were synthesized by solvothermal method in a Pyrex tube at 120 °C for 3 days.

2.1 Synthesis of TpaTfa[2]:

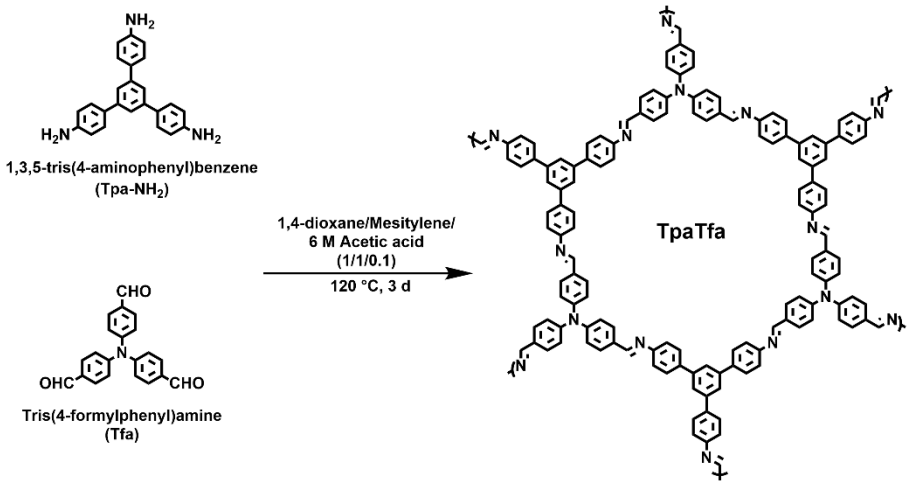

A Pyrex glass tube (15 mL) was charged with 1,3,5-tris(4-aminophenyl)benzene (Tpa-NH_2) (70.3 mg, 0.2 mmol), tris(4-formylphenyl)amine (Tfa) (65.9 mg, 0.2 mmol), 3 mL dioxane, 3 mL mesitylene and 0.3 mL 6 M acetic acid aqueous solution. The tube was first sonicated for 30 minutes and then flash frozen at 77 K (liquid N_2 bath) and degassed by three times of freeze-pump-thaw cycles. The internal pressure was evacuated to 10^{-3} mbar. The tube was sealed and placed in a preheated oven at 120 °C for 3 days. After finishing heating, the tube was cooled down and cut. The formed yellow precipitate was filtered and washed with acetone several times. Finally, the powder was dried in a normal oven at 80 °C. Yield = 94.1 % (118 mg)

2.2 Synthesis of TtaTfa[3]:

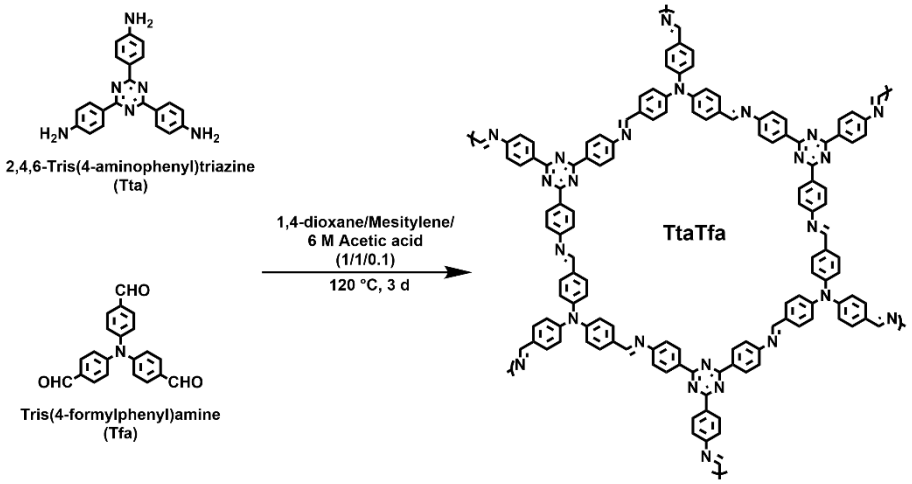

A Pyrex glass tube (15 mL) was charged with 2,4,6-Tris(4-aminophenyl)triazine (Tta) (70.9 mg, 0.2 mmol), tris(4-formylphenyl)amine (Tfa) (65.9 mg, 0.2 mmol), 3 mL dioxane, 3 mL mesitylene and 0.3 mL 6 M acetic acid aqueous solution. The tube was first sonicated for 1 hour to form yellow solid (polymer) and then flash frozen at 77 K (liquid N_2 bath) and degassed by three times of freeze-pump-thaw cycles. The internal pressure was evacuated to 10^{-3} mbar. The tube was sealed and heated at 120 °C for 3 days. The final bright yellow precipitate was washed with acetone several times and collected by filtration. Finally, the powder was dried in a normal oven at 80 °C. Yield = 87.3% (110 mg)

2.3 Synthesis of TtaTpa[4]:

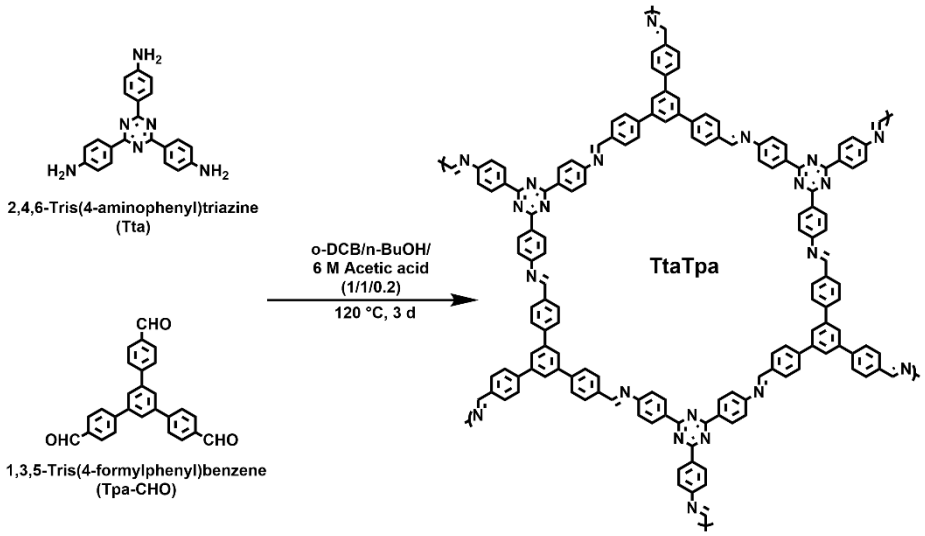

For the synthesis of TtaTpa, the solvent is different from the previous synthesis. A Pyrex glass tube (15 mL) was charged with 2,4,6-Tris(4-aminophenyl)triazine (Tta) (53.2 mg, 0.15 mmol), 1,3,5-Tris(4-formylphenyl)benzene (Tpa-CHO) (58.6 mg, 0.15 mmol), 2 mL o-DCB, 2 mL n-BuOH and 0.4 mL 6 M acetic acid aqueous solution. The tube was first sonicated for 30 minutes to form bulk solid and then flash frozen at 77 K (liquid N_2 bath) and degassed by three times of freeze-pump-thaw cycles. The internal pressure was evacuated to 10^{-3} mbar. The tube was sealed and heated at 120 °C for 3 days. The bright yellow precipitate was washed with acetone several times and collected by filtration. Finally, the powder was dried in a normal oven at 80 °C. Yield = 89.7 % (93 mg)

2.4 Ascorbic acid modification of the COFs

Typically, 30 mg of the pristine COF was stirred in 16 mL 0.1 M ascorbic acid aqueous solution for 5 minutes following by filtration and drying under ultra-high vacuum at room temperature overnight, to obtain AC modified COF.

Section S3. Photocatalytic H_2 evolution parameters

The photocatalysis was conducted in a 36 mL side irradiation quartz reactor equipped with a 152 mL glass gas container[5]. Generally, the COF was dispersed in either 16 mL 0.1 M ascorbic acid aqueous solution or TEOA/water (v:v=2 mL : 16 mL). Certain microliter H_2PtCl_6 aqueous solution (8 wt%) was added as the source of Pt cocatalyst. The reactor was sealed with rubber stoppers and degassed by Argon for 30 minutes prior to irradiation. Then, the reactor was irradiated with a 300 W Xe lamp ((L.O.T-Quantum design) with appropriate filters. The temperature of the system was kept at 20 °C by water circulating. Gas sample was taken from the headspace and H_2 was quantified by GC (Agilent 7820A) equipped with a thermal conductivity detector. The photocatalytic HER rates in ascorbic acid were determined from linear regression fit and the pressure increase was neglected in the calculations. Due to the negligible amount of H_2 evolved in TEOA and pure water, H_2 was only measured after finishing the irradiation. All the reacted COFs were recovered, washed with acetone and dried at 80 °C for further characterization.

Section S4. Characterization of the pristine COFs

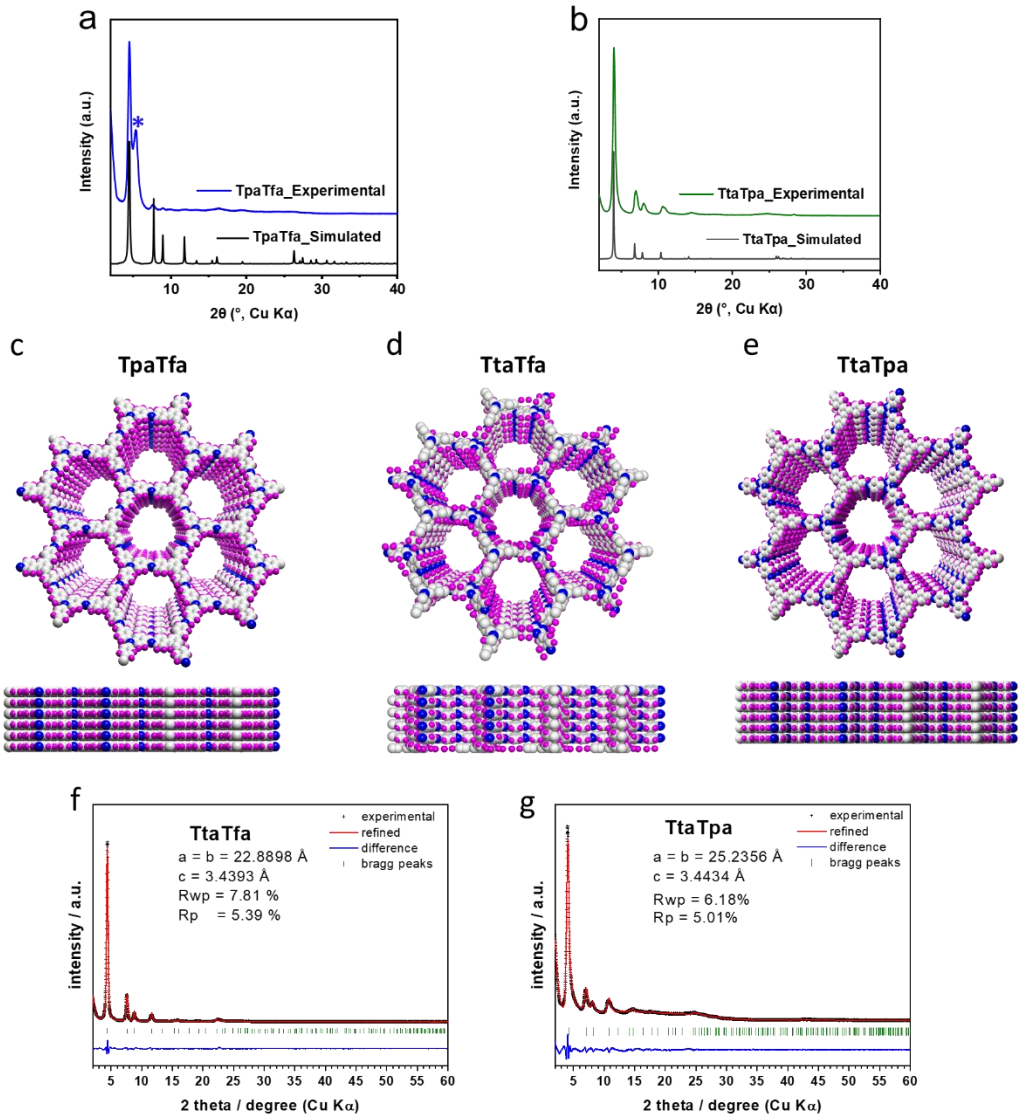

Figure S1. Experimental and simulated PXRD patterns of TpaTfa a) and TtaTpa b). (Diffraction peak marked with *can be probably attributed to a partial staircase-like stacking of the COF[6]). Crystal structures of TpaTfa c), TtaTfa d), and TtaTpa e). Top and side views of the three COFs showing the ideal eclipsed (AA) structures. Pawley refinement of f) TtaTfa, and g) TtaTpa.

The structural crystal models with **hcb** topology were constructed from the initially reported fractional coordinates in a *P*3 primitive hexagonal unit cell[2, 3, 4]. Geometry optimization of the structures with Universal Force Field (UFF) led to satisfactory models whose theoretical pattern matched well the experimentally obtained patterns in terms of reflection positions and relative intensities. The Pawley profile refinements were performed using a Pseudo-Voigt profile function. The observed diffraction patterns were subjected to a polynomial background subtraction and the refined parameters included the zero point shift, the unit cell parameters, the FWHM parameters and the peak asymmetry (Berar-Baldizzoni function). Due to the unknown peak, the crystal structure of TpaTfa was not refined.

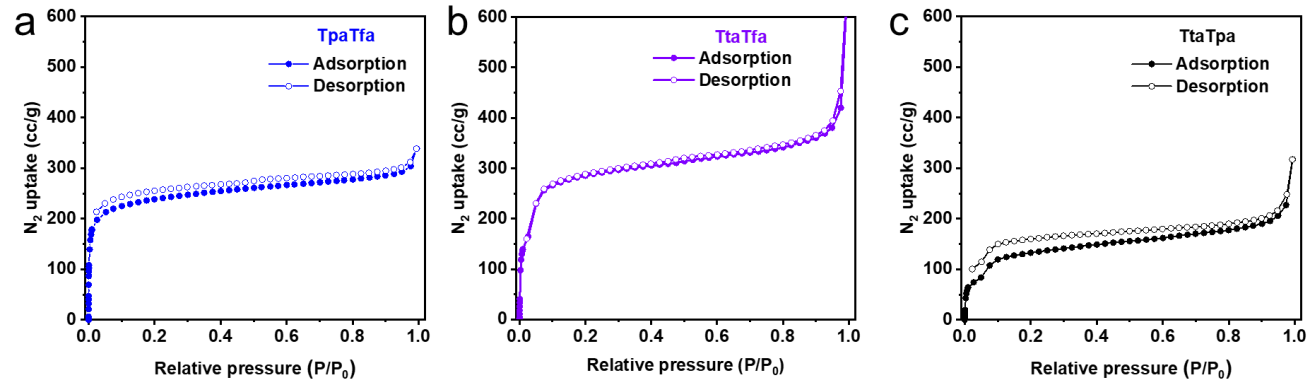

Figure S2. N_2 isotherms of a) TpaTfa b) TtaTfa, and c) TtaTpa.

The experimental BET surface areas of TpaTfa, TtaTfa, and TtaTpa derived from N_2 sorption are 938, 1135, and 508 $m^2 g^{-1}$, respectively. The simulated BET surface areas of TpaTfa, TtaTfa, and TtaTpa are 2300, 2245, and 2366 $m^2 g^{-1}$, respectively.

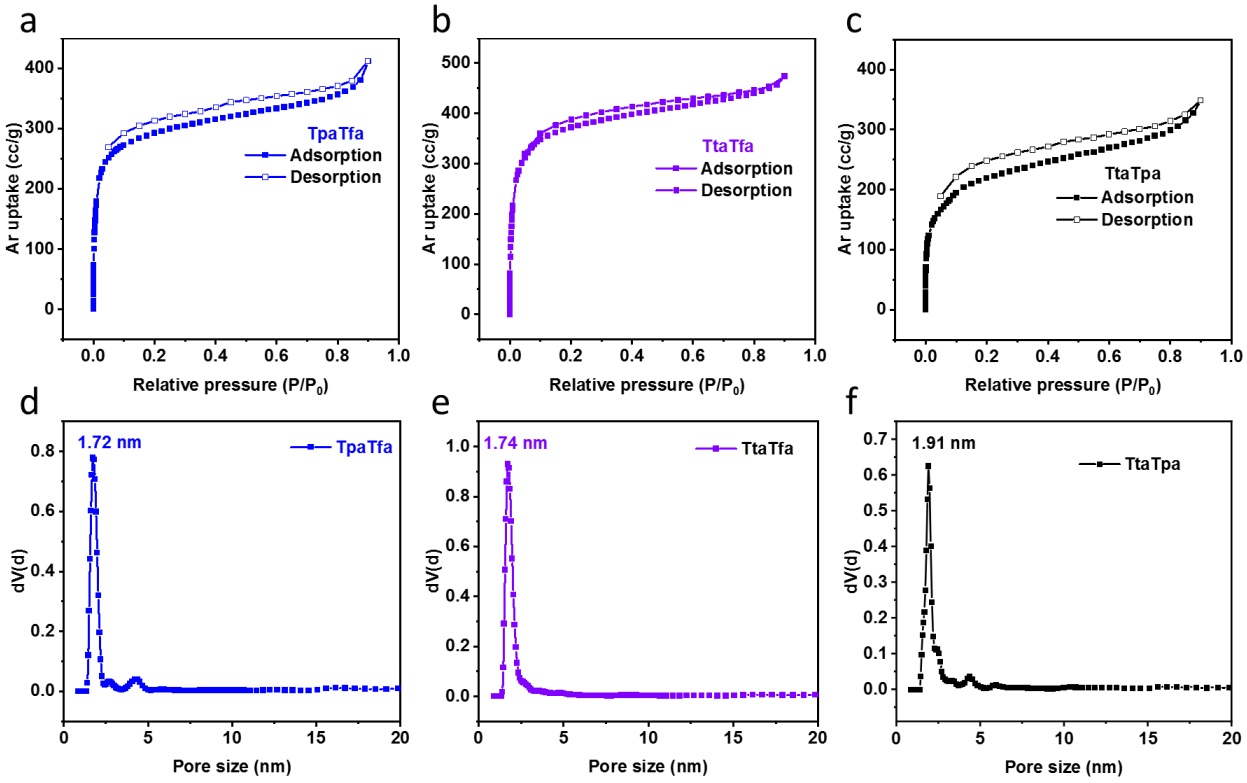

Figure S3. Argon isotherms (at 87K) of a) TpaTfa, b) TtaTfa and c) TtaTpa. Calculated pore size distribution plot of TpaTfa d) TtaTfa e) and TtaTpa f) from Argon isotherms at 87K after QSDFT model fitting of adsorption branch data.

The BET surface areas of TpaTfa, TtaTfa, and TtaTpa derived from Ar sorption were calculated to be 972, 1258, and 747 $m^2 g^{-1}$, respectively. Fitted with a quenched solid-state density functional theory (QSDFT) equilibrium model of Ar on carbon at 87 K (cylindrical pores) based on Ar isotherm, the experimental pore sizes were calculated to be 1.72, and 1.91 nm for TpaTfa and TtaTpa respectively. They are also identical to the theoretical pore size with 1.72 nm for TpaTfa and 2.3 nm for TtaTpa.

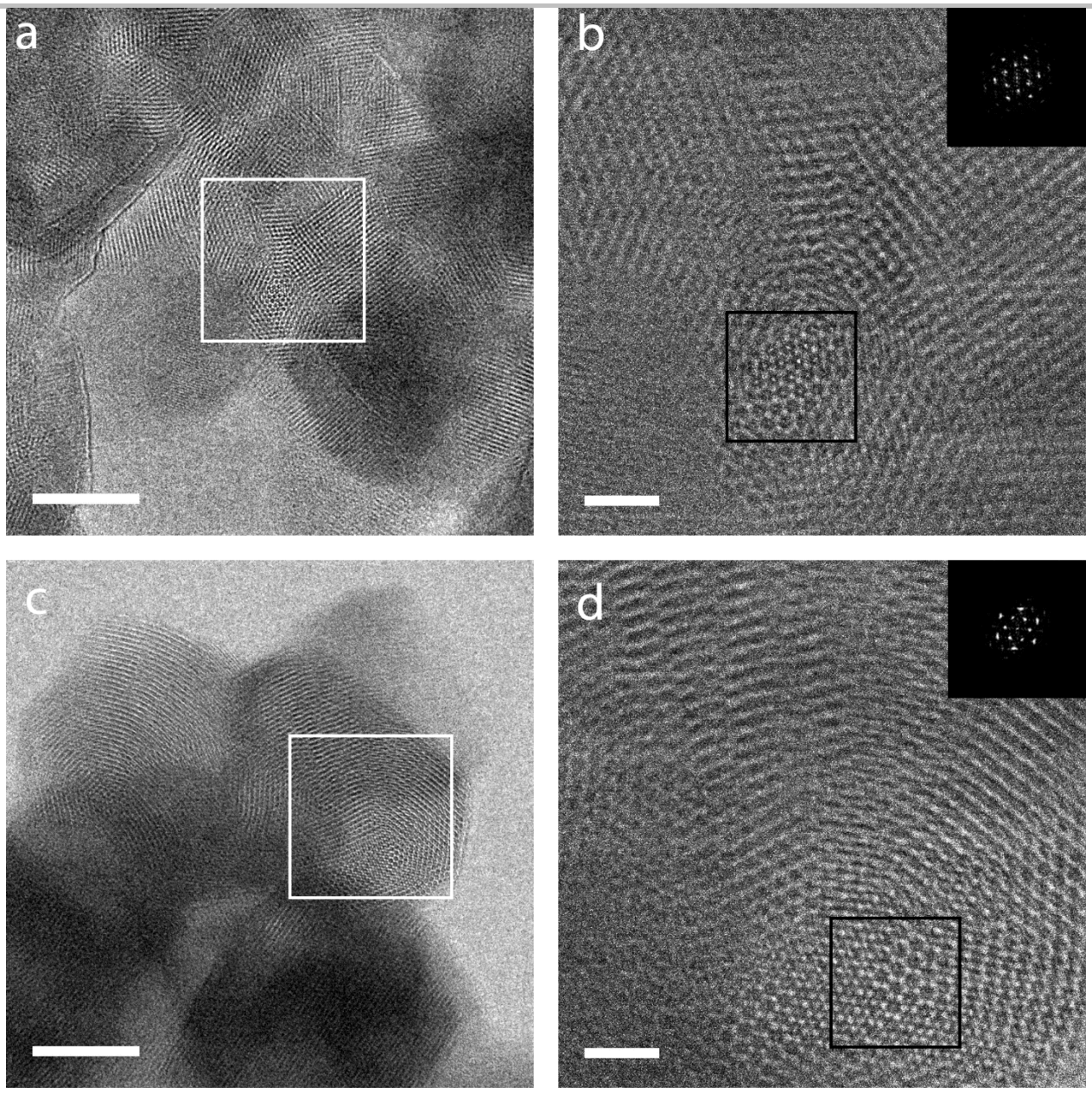

Figure S4. Low-dose TEM image of TpaTfa a) and TtaTpa c) under cryogenic conditions (scale bars, 50 nm). Low-dose HRTEM image of TpaTfa b) and TtaTpa d) under cryogenic conditions of the region indicated by white square in a) and c) (scale bar, 10nm). Insets in b) and d) show Fast Fourier Transforms (FFT) of the regions indicated by the black squares in the respective images.

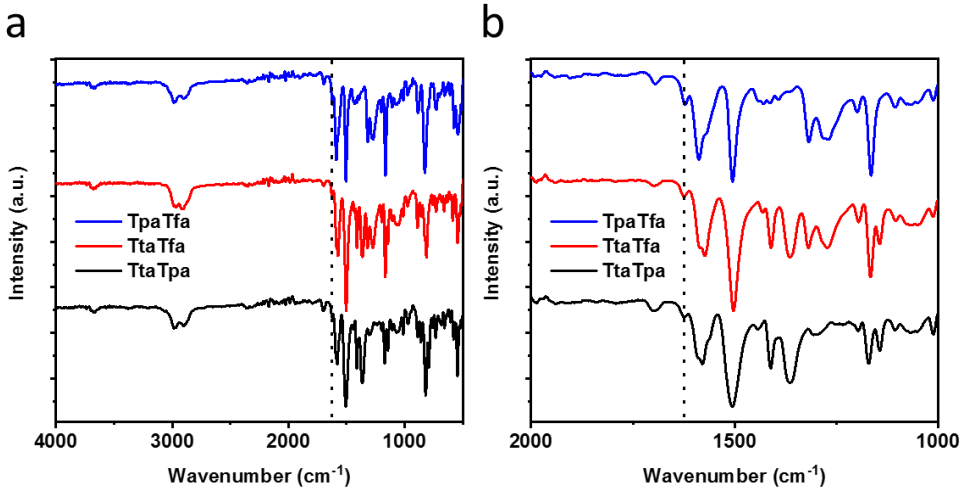

Figure S5. FT-IR spectra of TpaTfa, TtaTfa and TtaTpa. a) Full spectra. b) Enlarged view from 1000 cm^{-1} - 2000 cm^{-1}.

The prominent peaks at a wavenumber of around 1623 cm^{-1}, confirmed the successful formation of imine bonds, while the almost disappearance of peaks at 1693-1696 cm^{-1} (terminal aldehyde) and 2886-2985 cm^{-1} (terminal amine) verified the completion of the Schiff base reaction.

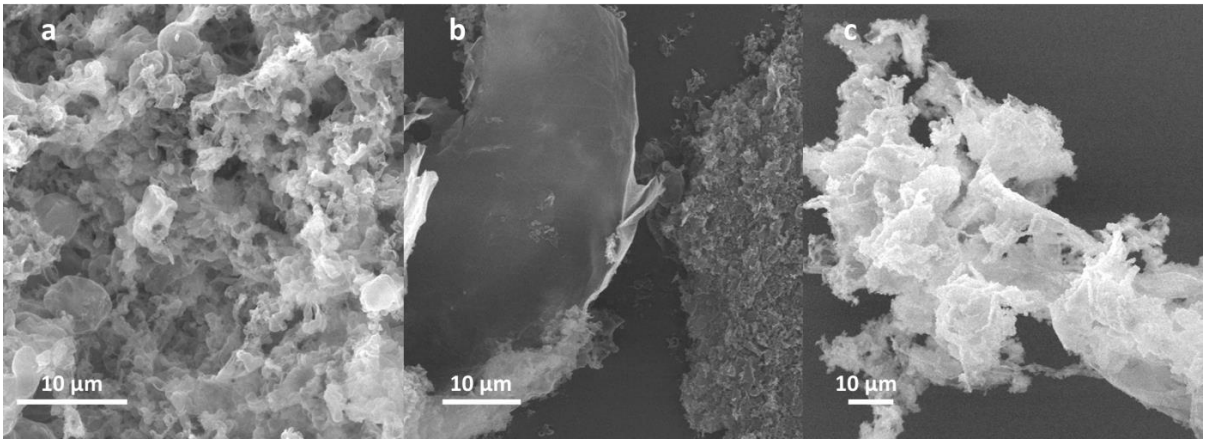

Figure S6. SEM images of TpaTfa a), TtaTfa b) and TtaTpa c).

Section S5. Confirmation and characterization of the protonated COFs

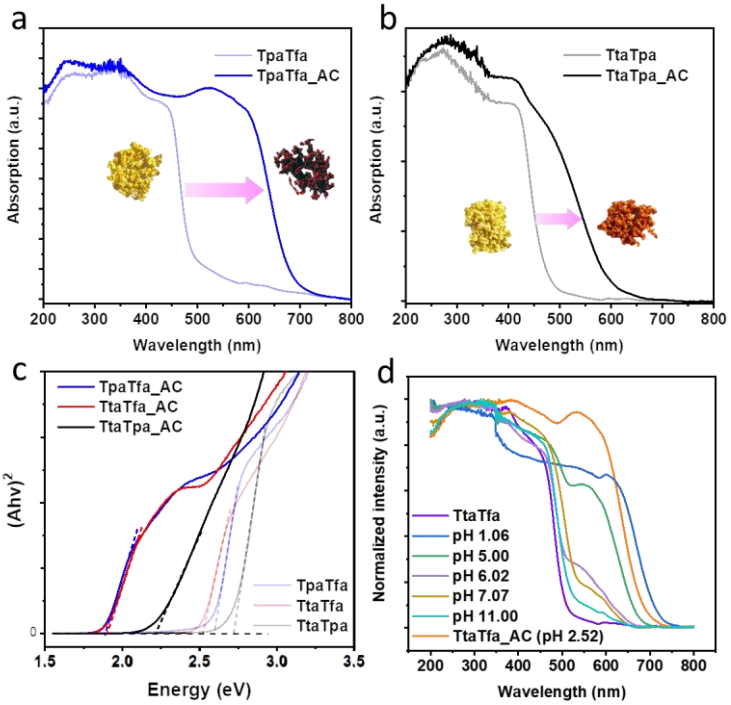

Figure S7. UV-Vis DRS spectra of TpaTfa a), TtaTpa b) before and after adding AC. The insets show the images of the corresponding COFs. c) Calculation of the band gap before and after AC modification. d) UV-Vis DRS spectra of TtaTfa at different pH values.

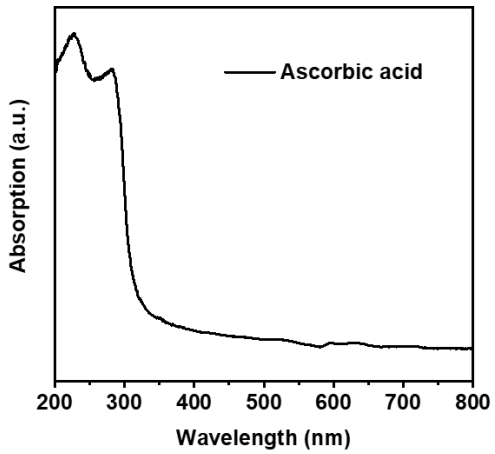

Figure S8. UV-Vis diffuse reflectance spectra of ascorbic acid.

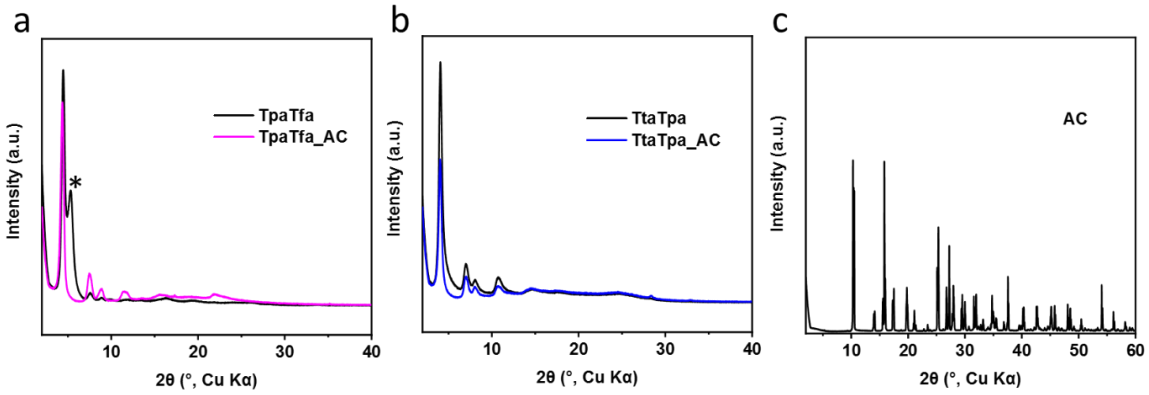

Figure S9. The experimental PXRD pattern of TpaTfa a), TtaTpa b) before and after ascorbic acid (AC) modification. c) The experimental PXRD of ascorbic acid. (Diffraction peak marked with *can be probably attributed to a partial staircase-like stacking of the COF[6]. Note that after protonation this peak disappeared, indicating a complete AA stacking)

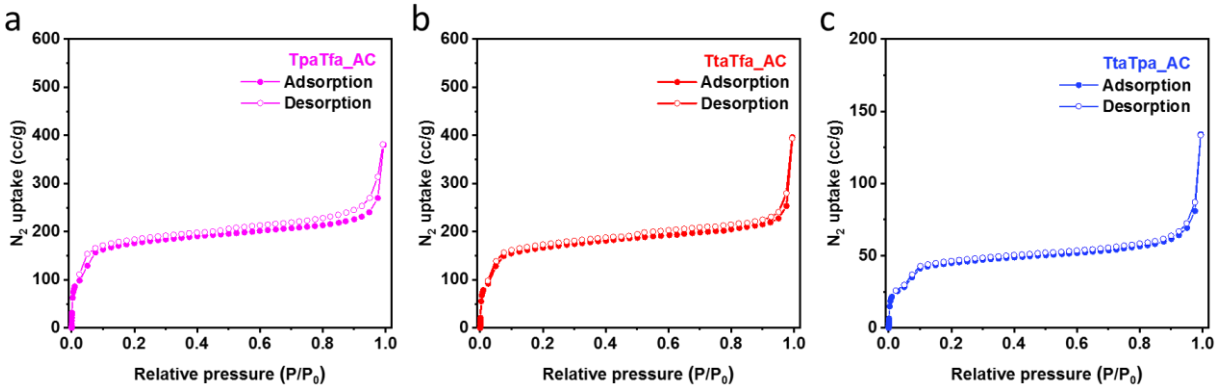

Figure S10. N_2 isotherms of the COFs after AC modification. a) TpaTfa_AC, b) TtaTfa_AC and c) TtaTpa_AC.

Modification by ascorbic acid leads to the decrease of the porosity. The BET surface area of TpaTfa_AC, TtaTfa_AC and TtaTpa_AC were measured to be 688 $m^2 g^{-1}$, 665 $m^2 g^{-1}$, 174 $m^2 g^{-1}$.

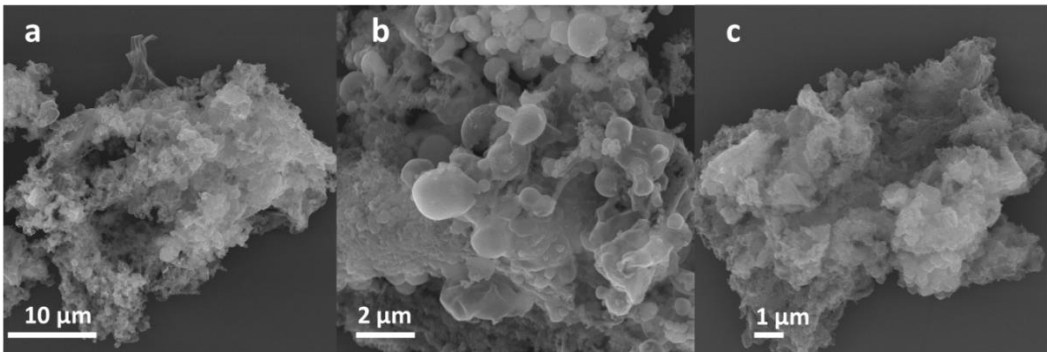

Figure S11. SEM images of the COFs after AC treatment. a) TpaTfa_AC, b) TtaTfa_AC and c) TtaTpa_AC.

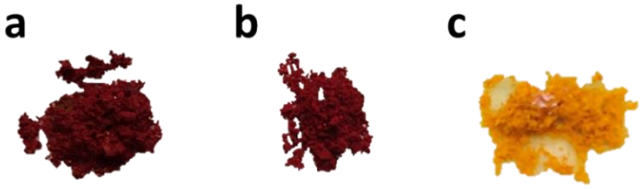

Figure S12. Photographs of TpaTfa a), TtaTfa b) and TtaTpa c) modified by Hydrochloric acid (HCl).

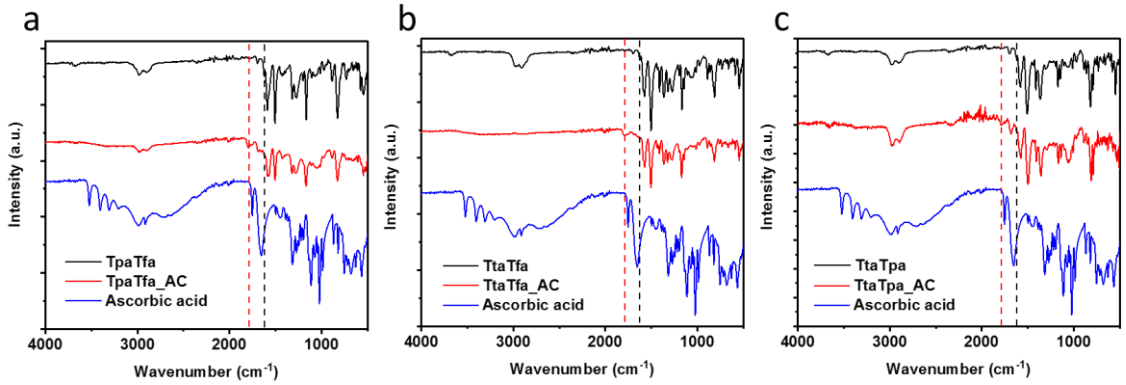

Figure S13. Full spectra comparison before and after AC modification, TpaTfa a), TtaTfa b) and TtaTpa c).

Table S1 Excitation energies for TtaTfa from experiment and theory.

	experimental	calculated CAM-B3LYP/ def2-SVP		
	UV-Vis DRS	HOMO-LUMO gap	1st excitation	1st excitation [a]
TtaTfa	2.45 eV (507 nm)	5.52 eV (225 nm)	3.56 eV (348 nm)	3.72 eV (334 nm)
TtaTfa+H$^+$	1.80 eV (688 nm) [b]	2.13 eV (583 nm)	1.74 eV (711 nm)	2.40 eV (518 nm)
TtaTfa+6H$^+$		3.72 eV (334 nm)	2.54 eV (488 nm)	2.64 eV (469 nm)

[a] Disregarding (nearly) "dark" excitations with oscillator strengths lower than 0.002. For TtaTfa, there are two degenerate states at 334 nm with oscillator strengths of 5.93; for TtaTfa+H$^+$, the state at 518 nm has oscillator strength 1.03.

[b] Exact degree of protonation not determined.

In Table S1 we compare HOMO-LUMO gaps and lowest (dark and bright) TD-DFT excitation energies for TtaTfa, TtaTfa+H$^+$ and TtaTfa+6H$^+$ to the onset of measured UV-vis DRS spectra. Protonation is clearly seen to lead to a redshift in both diagnostics (HOMO-LUMO gaps and excitation energies).

While the calculation reflects the trend of a redshift of the absorption onset upon protonation by about 180 nm (last column in Tab.S1), the absolute values differ significantly from the ones derived from UV-Vis measurements. This is not unexpected as only a single hexagonal pore was used as cluster model for the calculations, and no defects / imperfections were considered. In fact, periodic models (on the PBE level of theory) provide a smaller gap when compared to cluster models (not shown).

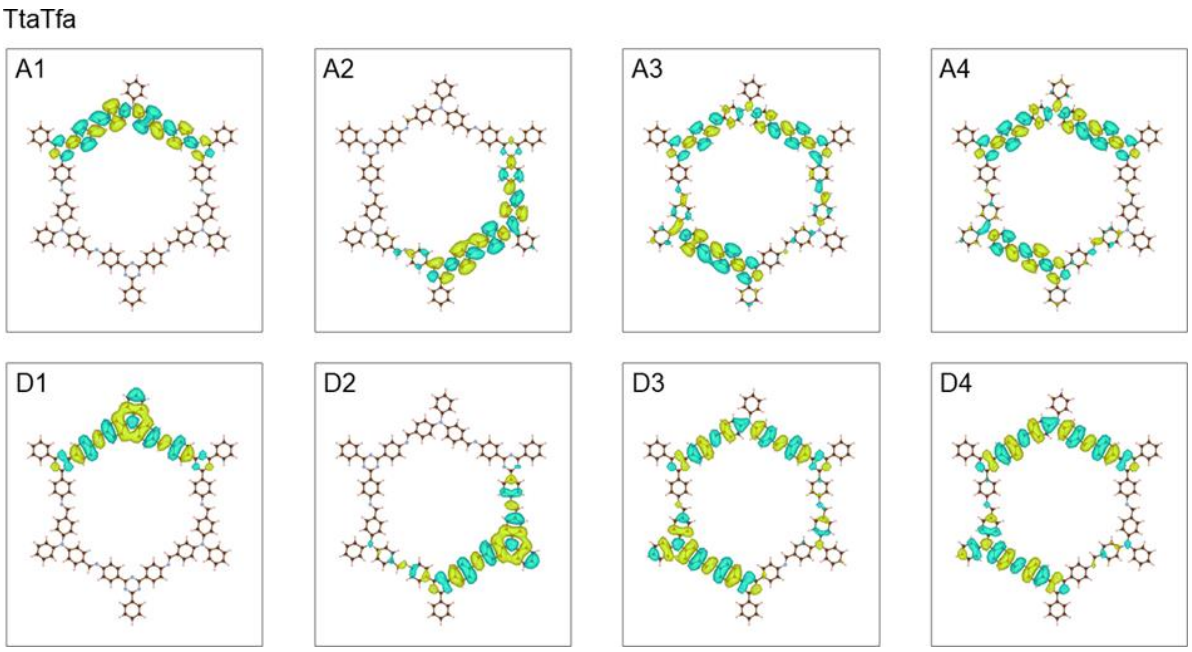

Figure S14. Natural transition orbitals (NTOs) for the lowest dipole-allowed excitation of TtaTfa. Donor and acceptor orbitals are denoted D and A, respectively, and ordered by their weights, which are 0.45, 0.27, 0.09 and 0.09, respectively. Large weights indicate a large contribution of the corresponding NTO pair to the transition.

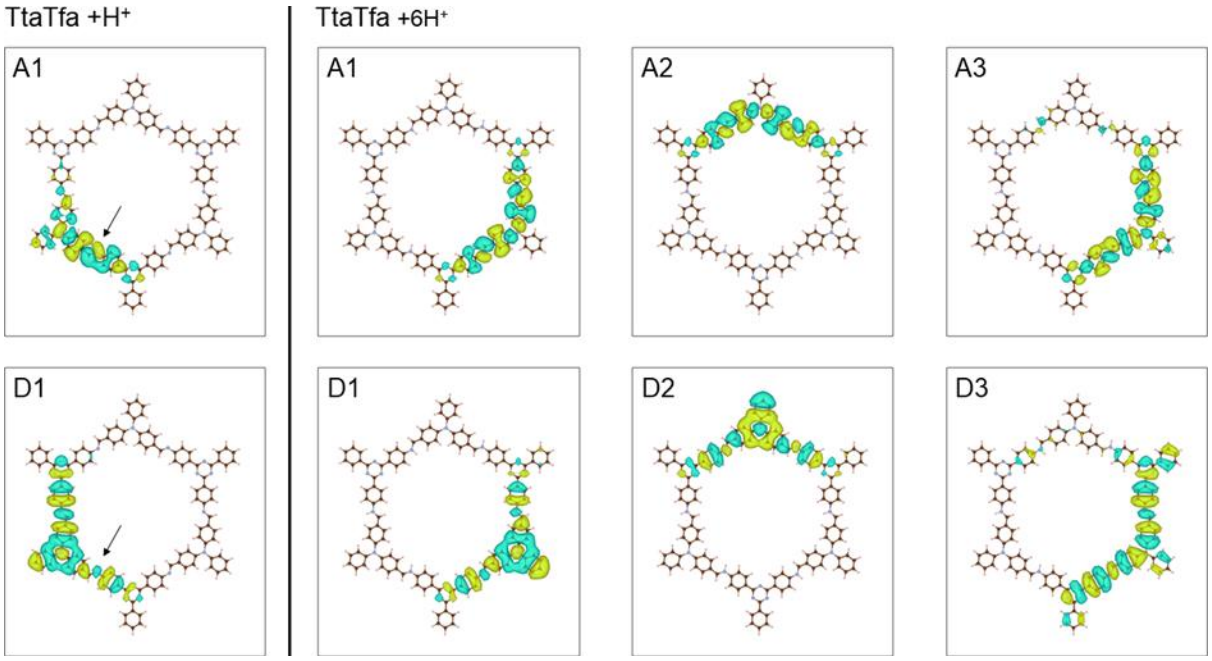

Figure S15. Natural transition orbitals (NTOs) for the lowest dipole-allowed excitation of protonated TtaTfa. The arrows indicate the protonation site for the singly protonated cluster. Donor and acceptor orbitals are denoted D and A, respectively, and ordered by their weights, which are 0.98 (single protonation, TtaTfa+H+) and 0.53, 0.39 and 0.03 (TtaTfa+6H+), respectively.

Section S6. Photocatalytic results

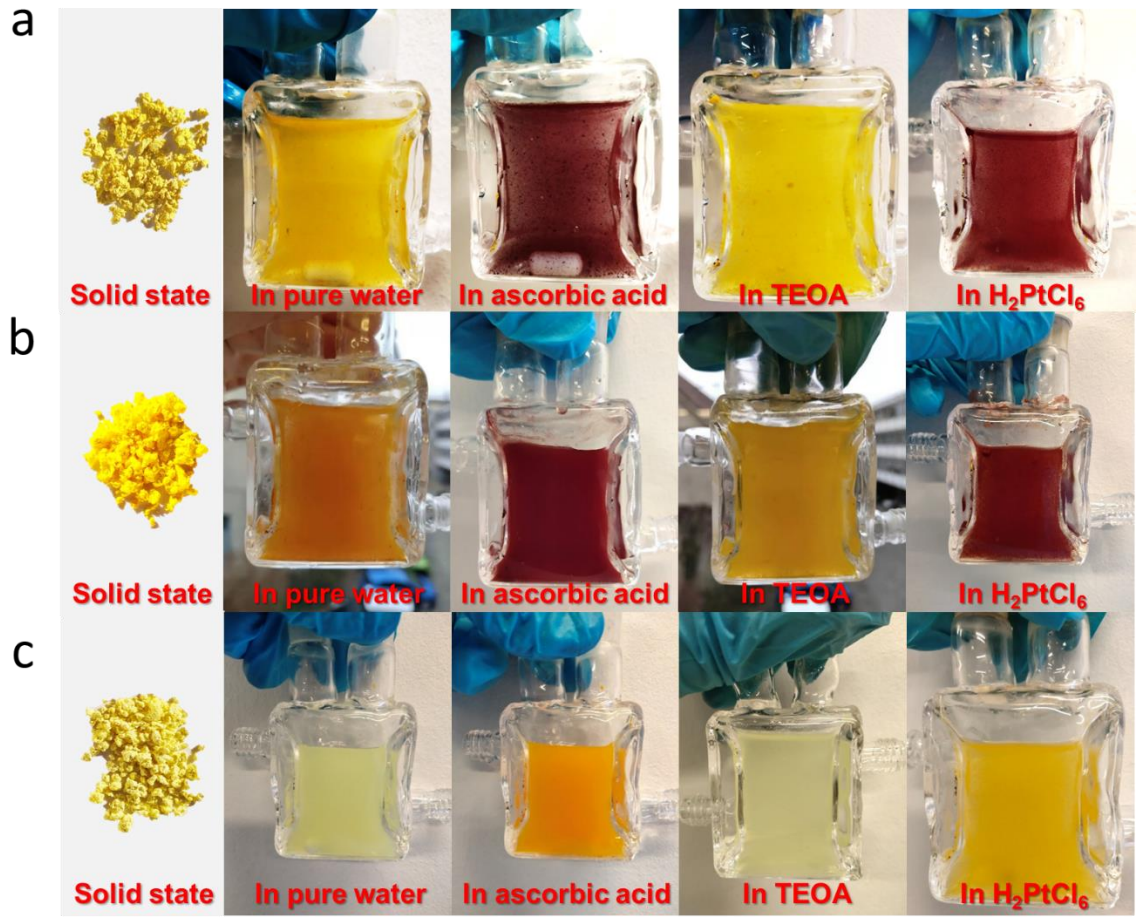

Figure S16. Color change at solid state, in pure water, in 0.1 M ascorbic acid (with 3 μL H_2PtCl_6), in 11 vol% TEOA (with 5 μL H_2PtCl_6), and in 3 μL H_2PtCl_6 aqueous solutions. a) TpaTfa, b) TtaTfa, c) TtaTpa.

Table S2 Comparison of photocatalytic HER performance of imine and imine related COFs.

Linkage	Catalyst	Sacrificial agent	pH	Activity (mmol g^{-1} h^{-1})	Amount Photocatalyst (mg)	Activity (μmol h^{-1})	AQE %	Light source	Ref.
Imine	TtaTfa	AC	Unadjusted	20.7	3	62.10	1.43 (450 nm)	>420 nm	This work
		TEOA		-	5	-	-		
	TpaTfa	AC		14.9	3	44.70	-		
		TEOA		-	5	-	-		
	TtaTpa	AC		10.8	3	32.40	-		
		TEOA		Negligible	5	-	-		
	Py-CITP-BT	AC	Unadjusted	8.875	20	177.50	8.45 (420 nm)	>420 nm	[7]
	Py-FTP-BT			2.875	20	57.50	-		
	Py-HTP-BT			1.078	20	21.56	-		
	PyTA-BC	AC	Unadjusted	5.03	1	5.03	1.46 (420 nm)	>420 nm	[8]
		TEOA/TEA		Negligible	1	-	-		
	PyTA-BC-Ph	AC		2.763	1	2.763	1.83 (420 nm)		
		TEOA/TEA		Negligible	1	-	-		
	PyTz-COF	AC	Unadjusted	2.07	35	96.71	-	AM 1.5	[9]
Hydrazine and imine	N3-COF	AC	PBS pH 7	0.075**	5	0.38	-	>420 nm	[10]
		TEOA	PBS pH 7	1.703	5	8.52	0.44 (450 nm)		
	A-TEBPY	TEOA	Unadjusted	0.098	10	0.98	-	AM 1.5	[11]
	PTP-COF	TEOA	PBS pH 7	0.083	5	0.42	0.87 (420 nm)	AM 1.5	[12]
Hydrazone	TFPT-COF	Sodium ascorbate	Unadjusted	0.230	10	2.3	-	>420 nm	[13]
		TEOA		1.970	4	7.88	2.2 (420 nm)		
	TTR-COF	TEOA	Unadjusted	1.720	20	34.40	-	>420 nm	[14]
β-ketoenamine	FS-COF +WS5F	AC	Unadjusted	16.3	5	81.5	7.4 (420 nm)	>420 nm	[15]
	FS-COF	AC	Unadjusted	10.1	5	50.50	3.2 (420 nm)		
		TEOA	Unadjusted	-	5	-	-		
	NTU-BDA-THTA	Sodium ascorbate	PBS pH 7	1.127	10	11.27	-	>420 nm	[16]
	TpPa-1-COF	Sodium ascorbate	PBS pH 7	1.22	10	12.20	-	>420 nm	[17]
	TpDTz*	TEOA	8.5 (HCl Adjusted)	0.941	5	4.71	0.2 (420 nm)	AM 1.5	[18]
	NUS-55	TEA	Unadjusted	0.433	2	0.87	1.55 (450 nm)	>420 nm	[19]
	Diacetylene-COF	TEOA	Unadjusted	0.324	10	3.24	1.3 (420 nm)	>395 nm	[5]

* TpDTz used Ni-thiolate cluster as the co-catalyst. Besides TpDTz, all the work used Pt as the co-catalyst.

** Estimated value from the figure.

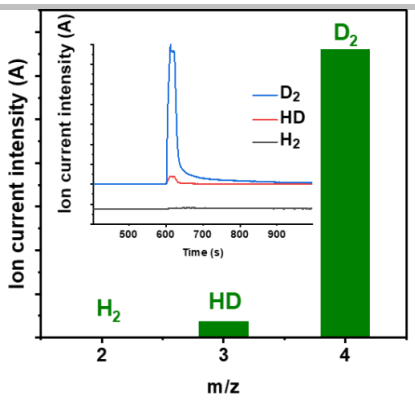

Figure S17. Hydrogen isotope labeling results (2 mg catalyst in 5 mL water, 2 µL H_2PtCl_6 (8 wt%, λ> 420 nm, irradiated for 30 minutes).

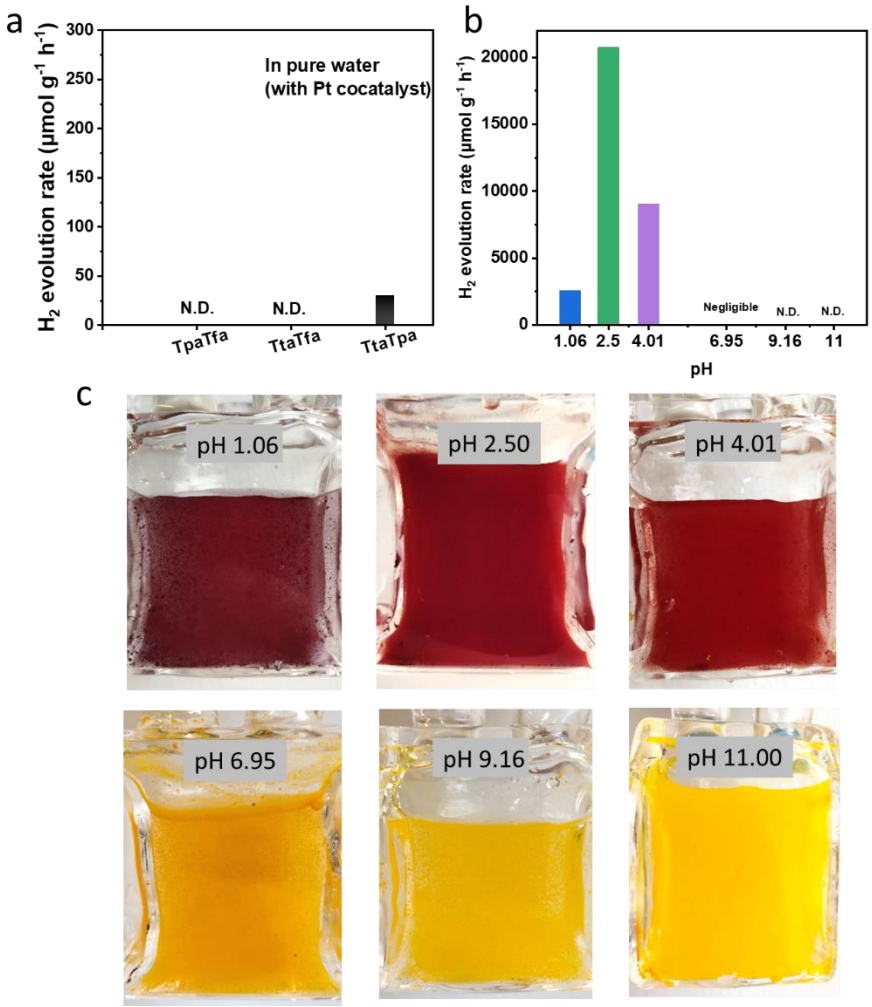

Figure S18. a) Photocatalytic H_2 evolution rate in pure water in presence of H_2PtCl_6 (5 mg catalyst in 16 mL water, 5 µL H_2PtCl_6 (8 wt%), λ> 420 nm, irradiated for 5 hours, 20 °C). b) comparison of the photocatalytic H_2 evolution rate at various pH-values c) Photographs of dispersion of TtaTfa-COF at various pH values. The pH was adjusted using diluted HCl and NaOH. pH 6.95 is the pH-value of 16 mL 0.1 M sodium ascorbate with 3 µL H_2PtCl_6 (8 wt%).

Table S3 pH values under different conditions.

Conditions	Pure water	0.1 M AC	0.1 M AC 3 µL H_2PtCl_6	0.1 M AC 5 µL H_2PtCl_6	3 µL H_2PtCl_6	11 vol% TEOA
pH	6.07	2.52	2.50	2.45	3.93	10.65

All of them were measured after dispersing the entire component for photocatalysis in 16 mL water at room temperature (25 °C).

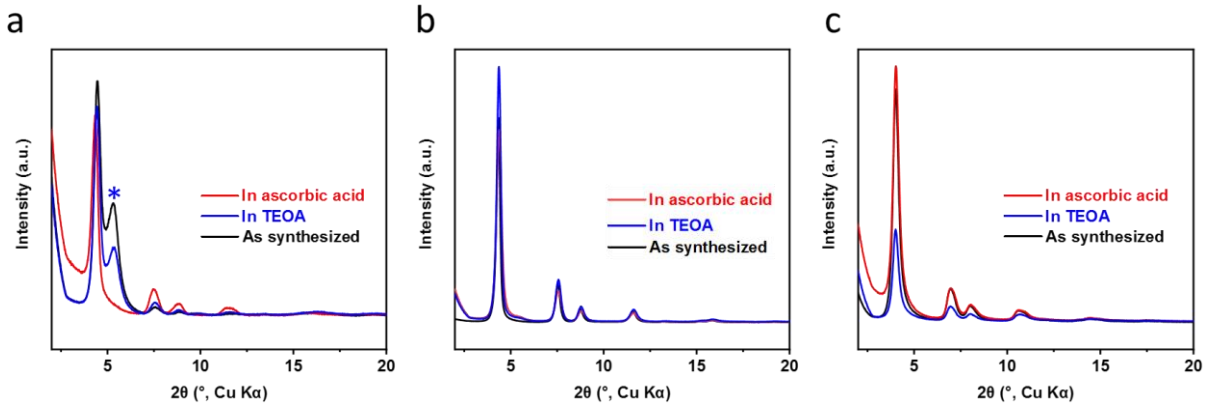

Figure S19. PXRD patterns of TpaTfa a), TtaTfa b) and TtaTpa c) after photocatalysis. (Recovered by filtration and washed by acetone and dried at 80 °C. Diffraction peak marked with * can be probably attributed to a partial staircase-like stacking of the COF[6-7])

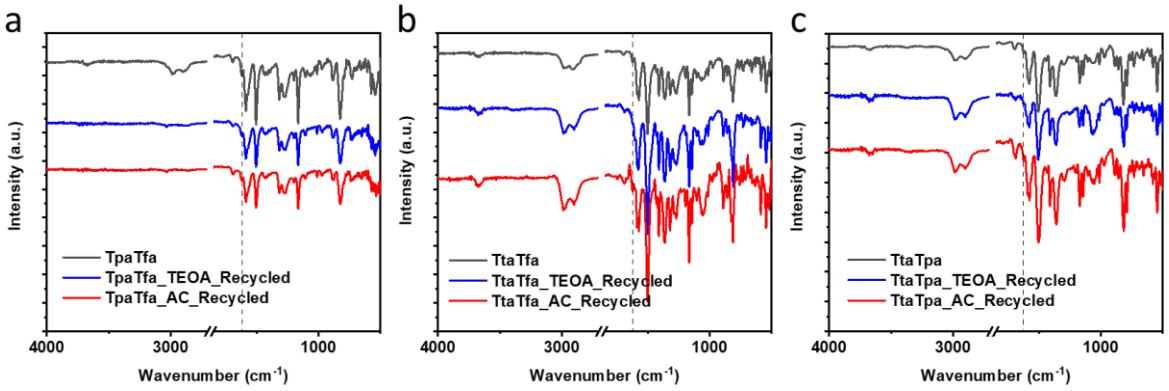

Figure S20. FTIR spectra comparison of the imine COFs before and after 4-hours photocatalysis.

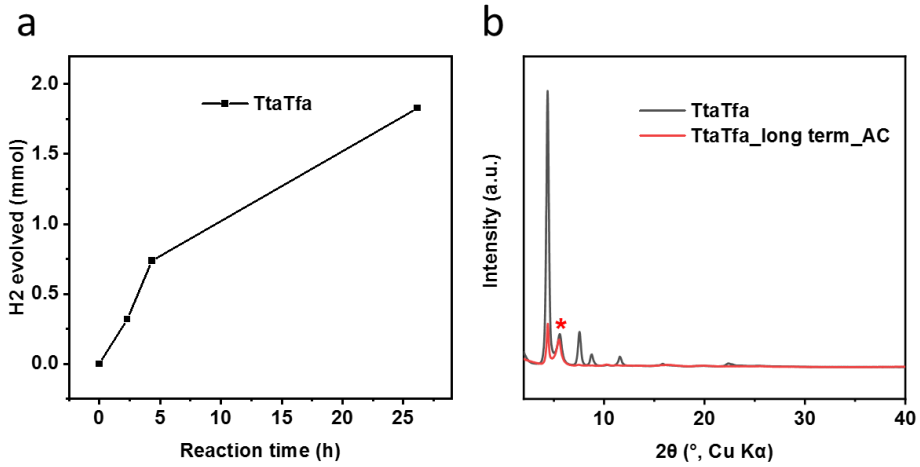

Figure S21. Long-term photocatalysis. a) Time course of photocatalytic H_2 evolution for TtaTfa. b) PXRD patterns of TtaTfa after Long-term photocatalysis. (Recovered by filtration and washed by acetone and dried at 80 °C. Diffraction peak marked with *can be probably attributed to a partial staircase-like stacking of the COF[6-7]).

Section S7. Mechanism study

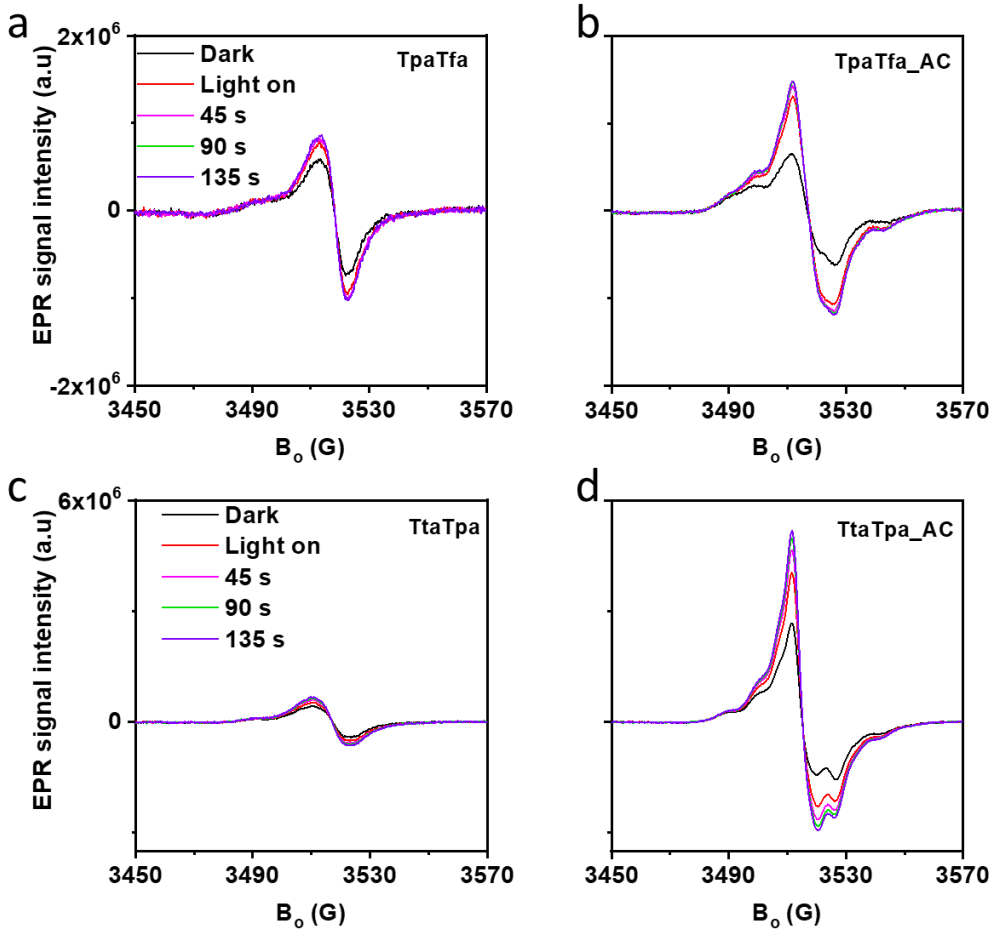

Figure S22. EPR conduction band electrons spectra (CB e^-) of TpaTfa a), TpaTfa_AC b) and TtaTpa c), TtaTpa_AC d) under dark condition and during visible light irradiation.

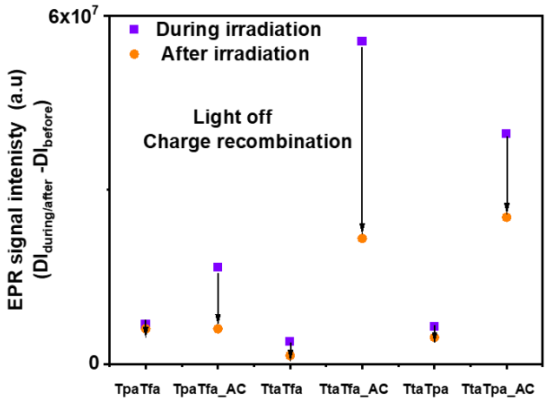

Figure S23. Comparison of the EPR CB e^- signal before and after visible light irradiation. This characterizes the recombination processes.

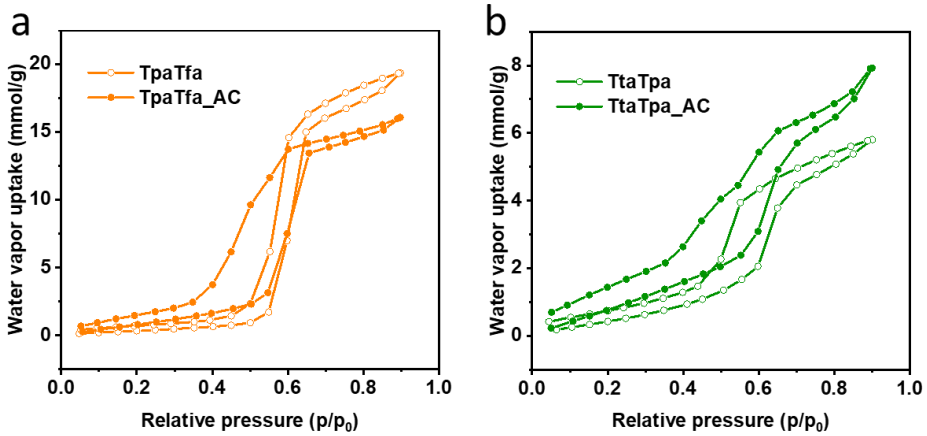

Figure S24. Water sorption analysis on TpaTfa, TpaTfa_AC a) and TtaTpa, TtaTpa_AC b) at 298 K.

Although the total water uptake at p/p_0 = 0.9 of TpaTfa_AC is smaller than TpaTfa, there is much more uptake at lower relative pressures. At p/p_0 = 0.2 (298 K), the water uptakes of TpaTfa_AC and TpaTfa are 1.46 mmol g^{-1} and 0.68 mmol g^{-1}, respectively. TtaTpa_AC shows the same trend as TtaTfa_AC, but TtaTpa_AC adsorbs more water both at p/p_0 = 0.2 and p/p_0 = 0.9 than TtaTpa. At p/p_0 = 0.2, the water uptakes of TtaTpa_AC and TtaTpa are 1.44 mmol g^{-1} and 0.74 mmol g^{-1}, respectively. At p/p_0 = 0.9, the water uptakes of TtaTpa_AC and TtaTpa are 7.92 mmol g^{-1} and 5.80 mmol g^{-1}, respectively. All the water sorption data show that the protonated imine COFs are more hydrophilic than the pristine materials.

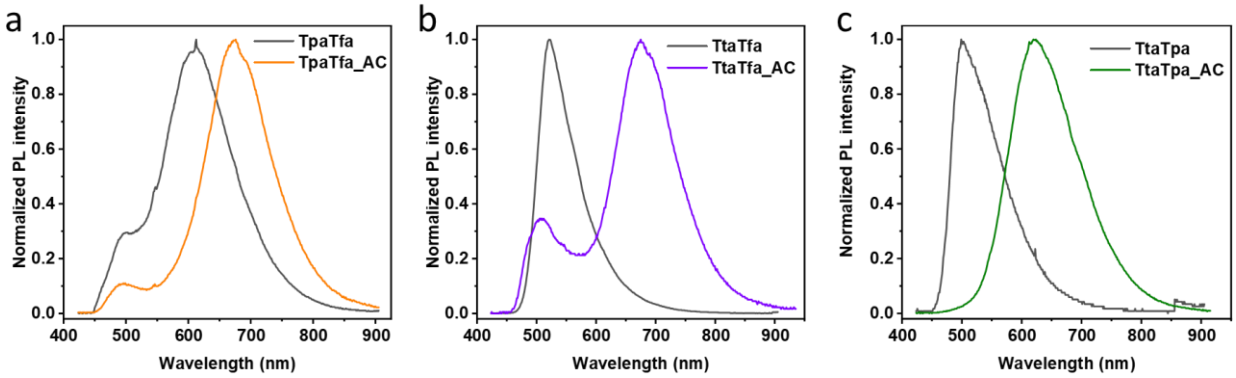

Figure S25. Photoluminescence (PL) spectra of TpaTfa a), TtaTfa b) and TtaTpa c)

The PL spectra of the samples were recorded b efore and after protonation in solid state. All the samples showed a red shift after protonation. This trend is consistent with the red shift of the light absorption upon protonation.

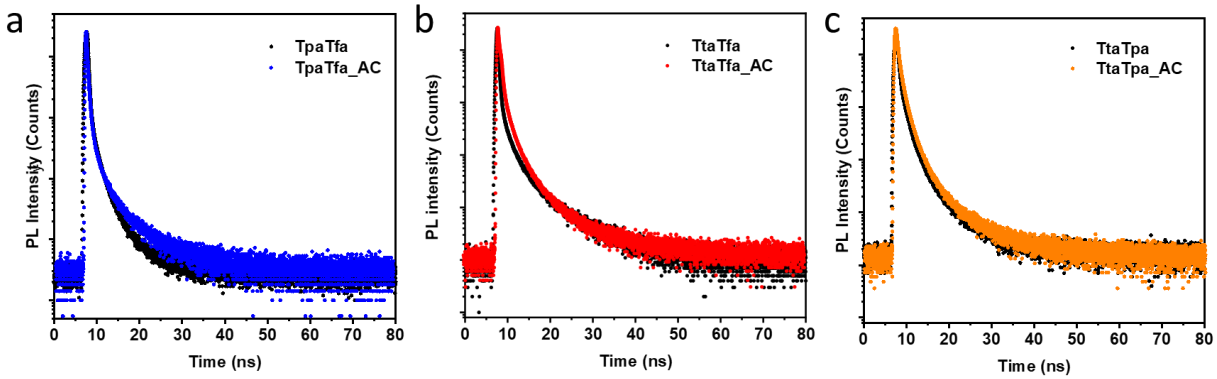

Figure S26. Time correlated single-photon counting of TpaTfa a), TtaTfa b) and TtaTpa c) before and after protonation.

Table S4. Summary of the fluorescence lifetime

	τ_1 (ns)	A_1	τ_2 (ns)	A_2	τ_3 (ns)	A_3	T_{avg} (ns)
TpaTfa	0.31	98.289 %	2.34	1.684 %	7.16	0.028 %	0.34
TpaTfa_AC	0.23	87.586 %	0.59	11.880 %	3.21	0.535%	0.29
TtaTfa	0.23	96.009 %	1.49	3.757 %	7.40	0.234 %	0.30
TtaTfa_AC	0.48	96.942 %	2.44	3.009%	10.01	0.050 %	0.54
TtaTpa	0.46	96.002 %	2.30	3.951 %	11.01	0.047 %	0.54
TtaTpa_AC	0.50	84.249 %	1.58	15.570%	7.96	0.181%	0.68

Longer lifetime of the excited state could allow more of the photo-generated electrons and holes to participate in the photocatalytic reactions[20]. We also measured the decay of PL signal of the as synthesized imine COFs and the protonated COFs and calculated the PL lifetimes via fitting the decays with three-phase exponential decay function (Fig. S24, Table S3). The PL lifetimes did not differ significantly for pristine and protonated samples, which indicates that photocatalytic performance of the COFs is not limited by their PL lifetimes.

References:

[1] D. N. Mastronarde, *J. Struct. Biol.* **2005**, *152*, 36-51.
[2] L. P. Zhai, N. Huang, H. Xu, Q. H. Chen, D. L. Jiang, *Chem. Commun.* **2017**, *53*, 4242-4245.
[3] A. F. M. El-Mahdy, C. H. Kuo, A. Alshehri, C. Young, Y. Yamauchi, J. Kim, S. W. Kuo, *J. Mater. Chem. A* **2018**, *6*, 19532-19541.
[4] B. C. Patra, S. K. Das, A. Ghosh, K. A. Raj, P. Moitra, M. Addicoat, S. Mitra, A. Bhaumik, S. Bhattacharya, A. Pradhan, *J. Mater. Chem. A* **2018**, *6*, 16655-16663.
[5] P. Pachfule, A. Acharjya, J. Roeser, T. Langenhahn, M. Schwarze, R. Schomacker, A. Thomas, J. Schmidt, *J. Am. Chem. Soc.* **2018**, *140*, 1423-1427.
[6] a) N. Keller, M. Calik, D. Sharapa, H. R. Soni, P. M. Zehetmaier, S. Rager, F. Auras, A. C. Jakowetz, A. Gorling, T. Clark, T. Bein, *J. Am. Chem. Soc.* **2018**, *140*, 16544-16552; b) F. Haase, K. Gottschling, L. Stegbauer, L. S. Germann, R. Gutzler, V. Duppel, V. S. Vyas, K. Kern, R. E. Dinnebier, B. V. Lotsch, *Mater. Chem. Front.* **2017**, *1*, 1354-1361.
[7] W. B. Chen, L. Wang, D. Z. Mo, F. He, Z. L. Wen, X. J. Wu, H. X. Xu, L. Chen, *Angew. Chem. Int. Ed.* **2020**, *59*, 16902-16909.
[8] A. F. M. El-Mahdy, A. M. Elewa, S. W. Huang, H. H. Chou, S. W. Kuo, *Adv. Opt. Mater.* **2020**, *8*, 2000641.
[9] W. Li, X. Huang, T. Zeng, Y. A. Liu, W. Hu, H. Yang, Y. B. Zhang, K. Wen, *Angew. Chem. Int. Ed.* **2021**, *60*, 1869-1874.
[10] V. S. Vyas, F. Haase, L. Stegbauer, G. Savasci, F. Podjaski, C. Ochsenfeld, B. V. Lotsch, *Nat. Commun.* **2015**, *6*, 8508.
[11] L. Stegbauer, S. Zech, G. Savasci, T. Banerjee, F. Podjaski, K. Schwinghammer, C. Ochsenfeld, B. V. Lotsch, *Adv. Energy Mater.* **2018**, *8*, 1703278.
[12] F. Haase, T. Banerjee, G. Savasci, C. Ochsenfeld, B. V. Lotsch, *Faraday Discuss.* **2017**, *201*, 247-264.
[13] L. Stegbauer, K. Schwinghammer, B. V. Lotsch, *Chem. Sci.* **2014**, *5*, 2789-2793.
[14] L. Y. Li, Z. M. Zhou, L. Y. Li, Z. Y. Zhuang, J. H. Bi, J. H. Chen, Y. Yu, J. G. Yu, *Acs Sustain. Chem. Eng.* **2019**, *7*, 18574-18581.
[15] X. Y. Wang, L. J. Chen, S. Y. Chong, M. A. Little, Y. Z. Wu, W. H. Zhu, R. Clowes, Y. Yan, M. A. Zwijnenburg, R. S. Sprick, A. I. Cooper, *Nat. Chem.* **2018**, *10*, 1180-1189.
[16] H. Wang, C. Qian, J. Liu, Y. F. Zeng, D. D. Wang, W. Q. Zhou, L. Gu, H. W. Wu, G. F. Liu, Y. L. Zhao, *J. Am. Chem. Soc.* **2020**, *142*, 4862-4871.
[17] F. M. Zhang, J. L. Sheng, Z. D. Yang, X. J. Sun, H. L. Tang, M. Lu, H. Dong, F. C. Shen, J. Liu, Y. Q. Lan, *Angew. Chem. Int. Ed.* **2018**, *57*, 12106-12110.
[18] B. P. Biswal, H. A. Vignolo-Gonzalez, T. Banerjee, L. Grunenberg, G. Savasci, K. Gottschling, J. Nuss, C. Ochsenfeld, B. V. Lotsc, *J. Am. Chem. Soc.* **2019**, *141*, 11082-11092.
[19] J. Wang, J. Zhang, S. B. Peh, G. L. Liu, T. Kundu, J. Q. Dong, Y. P. Ying, Y. H. Qian, D. Zhao, *Sci. China Chem.* **2020**, *63*, 192-197.
[20] A. Indra, A. Acharjya, P. W. Menezes, C. Merschjann, D. Hollmann, M. Schwarze, M. Aktas, A. Friedrich, S. Lochbrunner, A. Thomas, M. Driess, *Angew. Chem. Int. Ed.* **2017**, *56*, 1653-1657.
[21] F. Neese, WIREs *Comput. Mol. Sci.* **2012**, 2, 73–78.
[22] J. P. Perdew, K. Burke, M. Ernzerhof, *Phys. Rev. Lett.* **1996**, *77*, 3865–3868.
[23] S. Grimme, J. Antony, S. Ehrlich, H. Krieg, *J. Chem. Phys.* **2010**, *132*, 154104.
[24] S. Grimme, S. Ehrlich, L. Goerigk, *J. Comput. Chem.* **2011**, *32*, 1456–1465.
[25] R. Krishnan, J. S. Binkley, R. Seeger, J. A. Pople, *J. Chem. Phys.* **1980**, *72*, 650–654.
[26] T. Yanai, D. P. Tew, N. C. Handy, *Chem. Phys. Lett.* **2004**, *393*, 51–57.
[27] P. J. Stephens, F. J. Devlin, C. F. Chabalowski, M. J. Frisch, *J. Phys. Chem.* **1994**, *98*, 11623–11627.
[28] A. D. Becke, *J. Chem. Phys.* **1993**, *98*, 5648–5652.
[29] C. Lee, W. Yang, R. G. Parr, *Phys. Rev. B* **1988**, *37*, 785–789.
[30] F. Weigend, R. Ahlrichs, *Phys. Chem. Chem. Phys.* **2005**, *7*, 3297.
[31] E. Runge, E. K. U. Gross, *Phys. Rev. Lett.* **1984**, *52*, 997–1000.
[32] R. L. Martin, *J. Chem. Phys.* **2003**, *118*, 4775–4777.